AGU PUBLICATIONS

Geophysical Research Letters

RESEARCH LETTER

10.1002/2016GL070567

**Key Points:**
- A concept of ITOT is proposed to monitor global ocean warming
- ITOT detects ocean warming by measuring travel time changes of internal tides
- ITOT based on satellite altimetry is feasible and useful

**Correspondence to:**
Z. Zhao,
zzhao@apl.washington.edu

**Citation:**
Zhao, Z. (2016), Internal tide oceanic tomography, *Geophys. Res. Lett.*, *43*, 9157–9164, doi:10.1002/2016GL070567.

Received 22 APR 2016
Accepted 18 AUG 2016
Accepted article online 22 AUG 2016
Published online 10 SEP 2016



# Internal tide oceanic tomography

**Zhongxiang Zhao**[1]

[1] Applied Physics Laboratory, University of Washington, Seattle, Washington, USA

**Abstract** A concept of internal tide oceanic tomography (ITOT) is proposed to monitor ocean warming on a global scale. ITOT is similar to acoustic tomography, but that work waves are internal tides. ITOT detects ocean temperature changes by precisely measuring travel time changes of long-range propagating internal tides. The underlying principle is that upper ocean warming strengthens ocean stratification and thus increases the propagation speed of internal tides. This concept is inspired by recent advances in observing internal tides by satellite altimetry. In particular, a plane wave fit method can separately resolve multiple internal tidal waves and thus accurately determines the phase of each wave. Two examples are presented to demonstrate the feasibility and usefulness of ITOT. In the eastern tropical Pacific, the yearly time series of travel time changes of the $M_2$ internal tide is closely correlated with the El Niño–Southern Oscillation index. In the North Atlantic, significant interannual variations and bidecadal trends are observed and consistent with the changes in ocean heat content measured by Argo floats. ITOT offers a long-term, cost-effective, environmentally friendly technique for monitoring global ocean warming. Future work is needed to quantify the accuracy of this technique.

## 1. Concept

More than 90% of the heat gain of the Earth's climate system is stored in the ocean [*Levitus et al.*, 2012]. Heat entering the ocean at the sea surface is redistributed at depth by various ocean processes such as mixing and advection [*Liang et al.*, 2015]. Most of the heat is stored in the upper 700 m layer, and about 10% goes into the abyssal ocean [*Purkey and Johnson*, 2010; *Wunsch and Heimbach*, 2014]. Previous studies have suggested the importance of monitoring ocean subsurface temperature in closing the Earth's heat budget [*Lyman et al.*, 2010; *Meehl et al.*, 2011; *Kosaka and Xie*, 2013; *Cazenave et al.*, 2014]. However, observations of ocean subsurface temperature and ocean heat content (OHC) on a global scale pose a great challenge to oceanographers and climate scientists. Historical shipboard observations are biased both in space and time [*Abraham et al.*, 2013; *Legler et al.*, 2015]. Since 2005, the Argo Program has been sampling the upper 2000 m of the global ocean uniformly using an array of ≈3500 automatic profiling floats [*Roemmich et al.*, 2009; *Riser et al.*, 2016]. Subsurface temperatures are also measured by XBT surveys and the OceanSITES Program [*Legler et al.*, 2015]. Yet our existing Global Ocean Observing System (GOOS) is far from adequate to monitor the vast three-dimensional global ocean. New techniques are needed to improve the GOOS [*Lindstrom et al.*, 2012]. For example, Argo floats capable of descending to 6000 m depth are under development to measure abyssal ocean warming [*Johnson and Lyman*, 2014].

About 40 years ago, ocean acoustic tomography was proposed to monitor global ocean warming [*Munk and Worcester*, 1976]. This technique infers ocean temperature changes from travel time changes of sound propagating within the ocean [*Munk et al.*, 1995]. On a basin scale, acoustic tomography is also called acoustic thermometry [*Dushaw et al.*, 2009a]. In field experiments, an array of sound sources and receivers is deployed to measure sound propagation along multiple raypaths [*Munk et al.*, 1995; *Dushaw et al.*, 2009a]. Compared to traditional in situ measurements, acoustic tomography has two main advantages. First, it suppresses the temperature perturbations caused by mesoscale processes, which are the major error sources in field thermometer measurements. Second, it measures basin-scale ocean warming following long-range sound transmission [*Munk and Forbes*, 1989]. Acoustic tomography has been employed in a series of field experiments [*Dushaw et al.*, 2009a, 2009b].

Here we propose a new tomographic technique which utilizes the long-range propagation of internal tides. This technique is called internal tide oceanic tomography (ITOT) in analogous to ocean acoustic tomography. Internal tides are internal gravity waves of tidal frequency, generated in tidal current-bottom interactions over

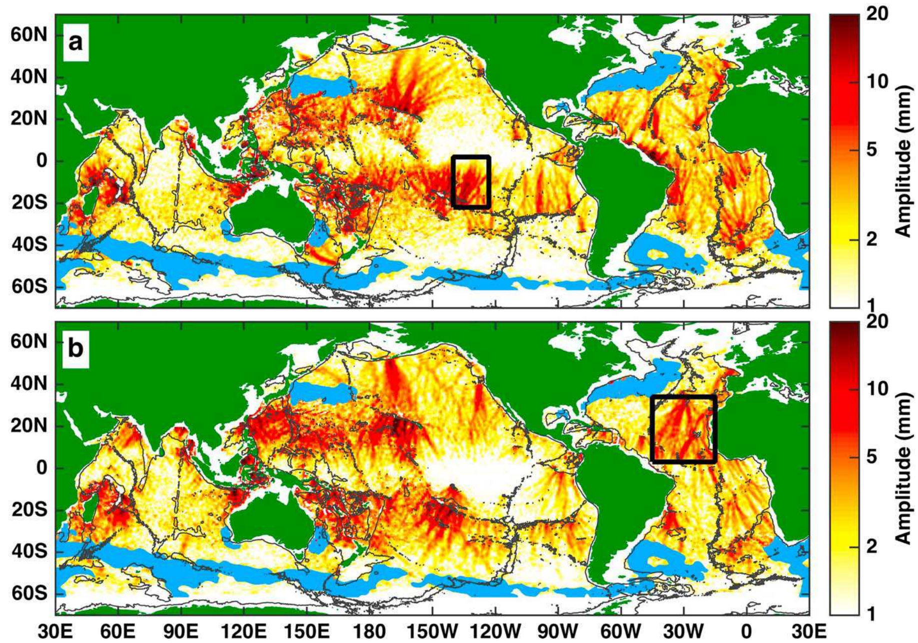


**Figure 1.** Global mode-1 $M_2$ internal tides observed using 20 years of multisatellite altimeter data from 1992 to 2012. Shown is the SSH amplitude. (a) Northbound component. (b) Southbound component. Blue patches denote regions where $M_2$ internal tides are overwhelmed by mesoscale contamination. The 3000 m isobaths are in black. Two black boxes denote the example regions shown in Figures 4 and 5.

topographic features. Low-mode internal tides may travel hundreds to thousands of kilometers [*Dushaw et al.*, 1995; *Ray and Mitchum*, 1996]. Upper ocean warming strengthens ocean stratification and thus increases the propagation speed of internal tides. Therefore, ocean temperature changes can be derived from the changes in the internal tide's propagation speed. Internal tides can be detected via their centimeter-scale sea surface height (SSH) fluctuations by satellite altimetry [*Ray and Mitchum*, 1996]. ITOT is inspired by recent advances in observing internal tides by satellite altimetry [*Zhao et al.*, 2016]. Figure 1 shows the global mode-1 $M_2$ internal tides, constructed using 20 years of multisatellite altimeter data. Long-range internal tidal beams occur widespread in the Pacific, Atlantic, and Indian Oceans. Here the internal tide field has been divided into northbound and southbound components, respectively [*Zhao et al.*, 2016]. This decomposition makes it possible to accurately track the long-range propagation of an internal tidal beam.

## 2. Two Main Challenges

### 2.1. How to Precisely Measure the Phase of Internal Tides?

The first challenge to the ITOT technique is how to precisely measure the phase of internal tides by satellite altimetry. In particular, the resultant phase information should be accurate enough to resolve the changes caused by global ocean warming. There are two particular difficulties. (1) The first difficulty stems from the complex nature of the global internal tide field. The numerous generation sites and long-range propagation of internal tides suggest that multiwave interference of some degree is widespread throughout the global ocean. Thus, the phase of internal tides obtained by pointwise harmonic analysis is distorted by multiwave interference and cannot be used to quantify the spatiotemporal variability of the phase. (2) The second difficulty arises from the low temporal and spatial sampling rates of altimeter satellites. To evaluate the internal tide's temporal variability, the internal tide field should be mapped using short time windows (Figure 2). However, internal tides extracted in short time windows (e.g., 1 year window) by pointwise harmonic analysis are overwhelmed by background noise, and their phases have large uncertainties.

A plane wave fit method has been employed to overcome these difficulties [*Zhao*, 2016; *Zhao et al.*, 2016]. Plane wave fitting is a variant of pointwise harmonic analysis and has been used to map the barotropic tide in coastal regions [*Munk et al.*, 1970]. In this method, internal tides are extracted using data in two-dimensional fitting windows, rather than at individual sites. A prerequisite wave number can be calculated using

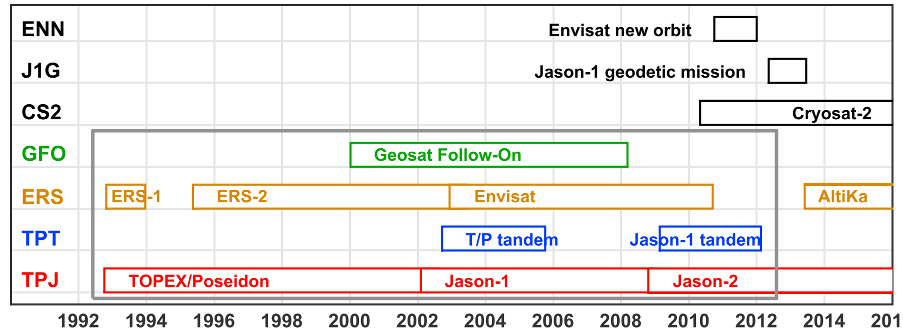


**Figure 2.** Temporal coverage of multisatellite altimeter data. The gray box denotes the 20 years of altimeter data used in *Zhao et al.* [2016]. The internal tide products shown in Figures 4 and 5 are using yearly data set of all available altimeter missions shown here.

climatological stratification profiles in the World Ocean Atlas 2013 (WOA13). To avoid repetition, interested readers are referred to *Zhao et al.* [2016] for a detailed description of this method.

This mapping technique well addresses the above challenges. (1) It separately resolves multiple internal waves of arbitrary propagation directions. As shown in Figure 1, the northbound and southbound internal tidal waves are obtained. Thus, the phase of one isolated internal tidal beam can be tracked to calculate travel time changes [*Zhao et al.*, 2016], which are inversely proportional to speed changes. (2) A fitting window of 250 km by 250 km contains about 3000 SSH data in 1 year for any single satellite altimeter. Thus, a 1 year time window provides sufficient independent data to guarantee robust plane wave fitting. This makes it possible to construct yearly internal tide fields from 1995 to 2014, when two or more altimeter satellites are in operation at the same time (Figure 2). The 95% confidence level in phase depends on the strength of internal tides and background noise level. It is about 5° for an internal tide with amplitude ≥5 mm based on our analyses in the North Pacific.

### 2.2. How to Derive Ocean Temperature Changes From the Internal Tide's Speed Changes?

Heat enters the ocean from the sea surface and is redistributed in the ocean interior; as a result, more heat is initially stored in the upper layer [*Levitus et al.*, 2012; *Wunsch and Heimbach*, 2014]. Figure 3b gives two warming profiles calculated from globally averaged Argo measurements using two distinct mapping methods [*Roemmich et al.*, 2015]. In our study, ocean warming is modeled following a normalized profile $t'(z)$ from Argo measurements (Figure 3b), and its magnitude at the sea surface $\Delta$ is to be determined from travel time changes of internal tides. The background stratification is calculated from a WOA13 climatological temperature profile $t(z)$ (Figure 3a). Assuming $t'(z)\Delta$ (i.e., the product of $t'(z)$ and $\Delta$) is the warming profile, then a warmed temperature profile is $t(z)+t'(z)\Delta$. The corresponding propagation speed can be calculated from the

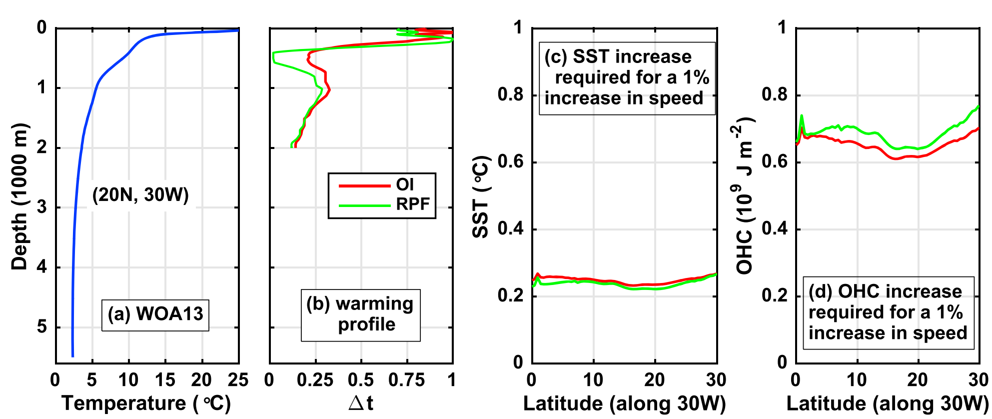


**Figure 3.** Conversion functions from the internal tide's speed change rates to the changes of SST (sea surface temperature) and OHC (ocean heat content). (a) A typical temperature profile from WOA13. (b) Normalized warming profiles from Argo measurements. Labels OI and RPF signify two different mapping methods (see Figure 2b in *Roemmich et al.* [2015]). (c) SST increase required for a 1% increase in the internal tide's propagation speed. (d) As in Figure 3c but for the OHC increase.

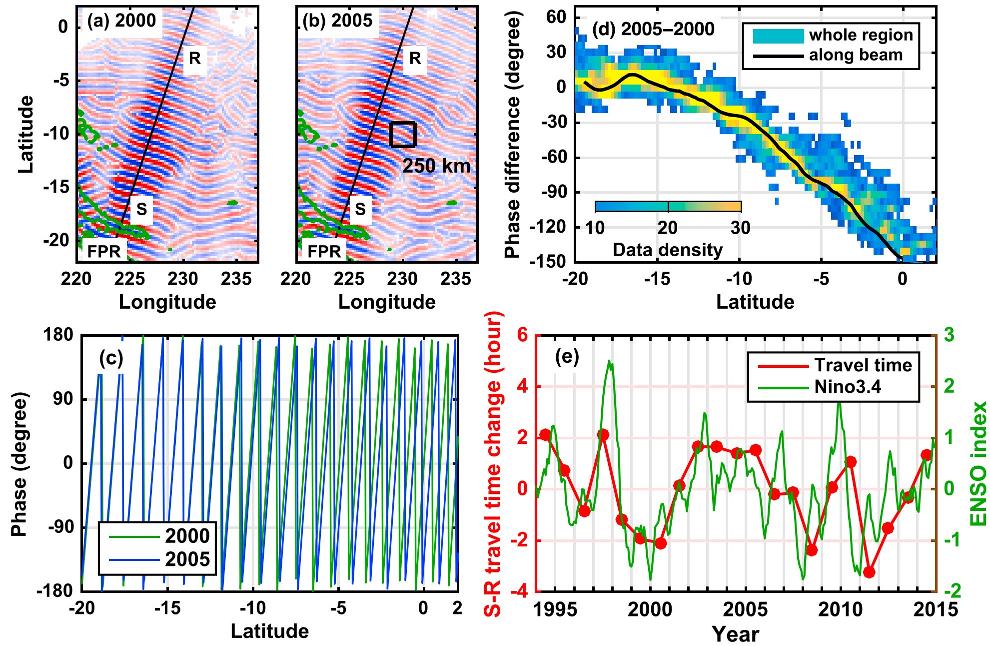


**Figure 4.** The northbound $M_2$ internal tides in the eastern tropical Pacific. See Figure 1a for location. An internal tidal beam originated at the French Polynesian Ridge travels over 2000 km. (a) The 2000 internal tide field. (b) The 2005 internal tide field. The black box shows a fitting window of 250 km by 250 km. (c) Along-beam Greenwich phase. (d) Phase differences between 2005 and 2000. The black line indicates phase differences along the beam. Colors indicate statistical distribution of phase differences in the whole region (in bins of 3° phase by 1° latitude). (e) Yearly time series of S-R travel time changes (positive means travel faster). It is highly correlated with the ENSO index (Nino3.4).

Sturm-Liouville eigenvalue equation [e.g., *Gill*, 1982]. Using the temperature profiles before and after warming, we can calculate a pair of phase speeds and a speed change rate Cp%. The ocean warming signals are small; therefore, both Cp% and Δ can be linearized, implying that they have a linear relation:

$$\Delta = \mathrm{Cp\%} \cdot \mathrm{F}(\mathrm{lon}, \mathrm{lat}, t'(z)), \tag{1}$$

where $\mathrm{F}(\mathrm{lon}, \mathrm{lat}, t'(z))$ is a function of location and the warming profile.

The relationship between Δ and Cp% can be interpreted as the sea surface temperature (SST) increase (i.e., Δ at the sea surface) required for a 1% increase in the speed of internal tides. In the North Atlantic, for both warming profiles shown in Figure 2b, the SST increase ranges from 0.2 to 0.25°C for the internal tide's speed increase by 1% (Figure 3c). Changes in OHC can be calculated from vertical integration, $\mathrm{OHC} = \int \rho c_p t'(z) \Delta \mathrm{d}z$, where $c_p$ is seawater heat capacity ($\sim 3.8 \times 10^3$ J kg$^{-1}$°C$^{-1}$), and $\rho$ is water density (1038 kg m$^{-3}$). It suggests that, for both warming profiles, 0.6–0.75×10$^9$ J m$^{-2}$ is required to increase the internal tide's speed by 1% (Figure 3d). This framework neglects minor contributions from salinity and currents, which will be quantified in future work.

## 3. Proof of Concept

### 3.1. An Example in the Eastern Tropical Pacific

Figure 4 shows the northbound $M_2$ internal tides in the eastern tropical Pacific constructed using yearly SSH data sets. An $M_2$ internal tidal beam is observed to propagate over 2000 km from the French Polynesian Ridge. The 2000 and 2005 internal tide fields have similar spatial patterns (Figures 4a and 4b). However, they have systematic phase biases (Figure 4c). Although there is no obvious phase difference in the source region (S), the phase difference in the receiver region (R) is about 120°, equivalent to 4 h in time. The phase difference increases with propagation distance, because the internal tide travels faster in 2005 (Figure 4c). The along-beam observation agrees well with the statistical distribution of phase differences in the whole domain 220–235°E, 20°S–2°N (Figure 4d). From a travel time change of 4 h and an S-R travel time of about 175 h (14 cycles; refer to Figure 4c), we obtain a travel time change rate of 2.3%.

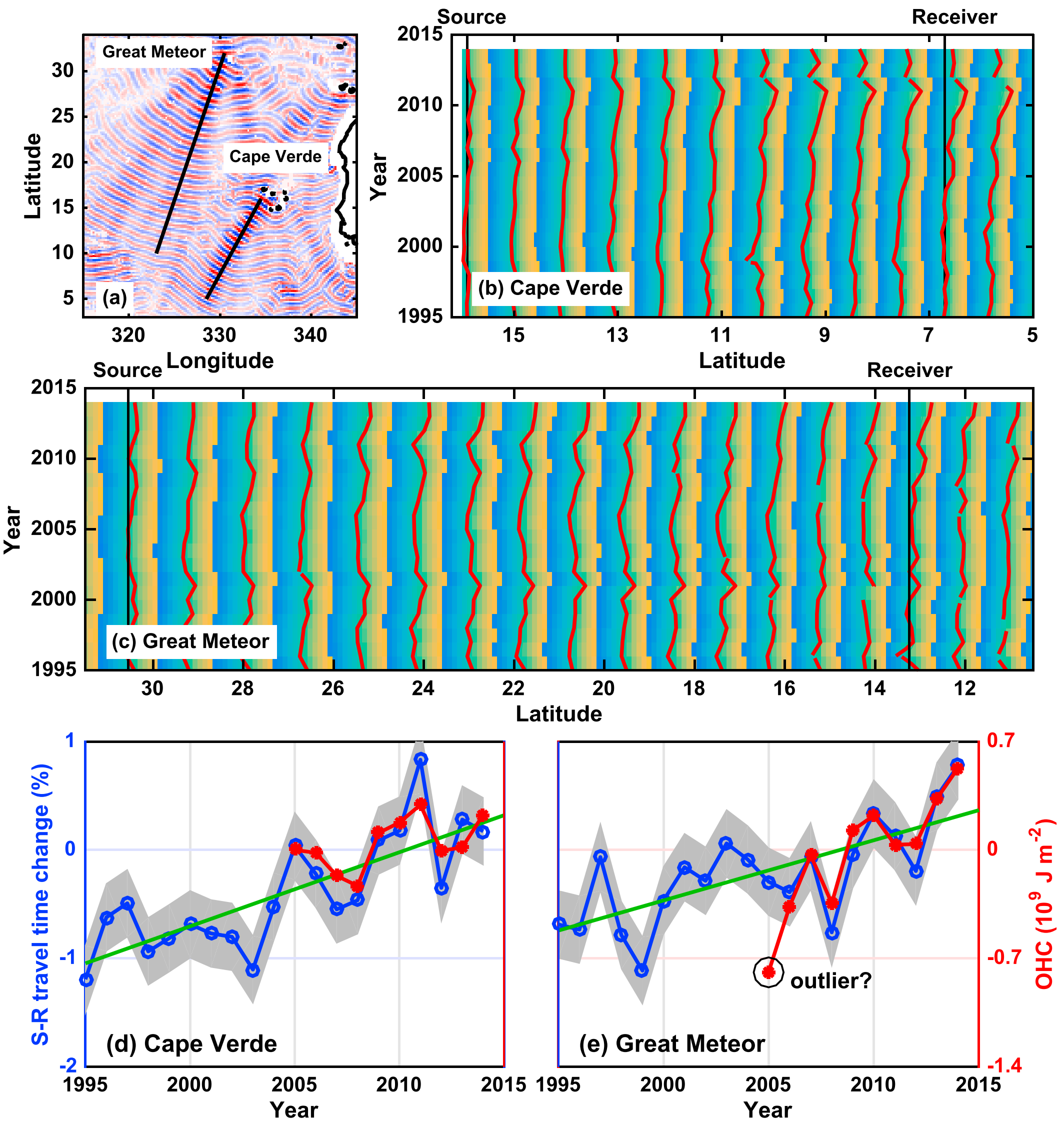


**Figure 5.** The southbound $M_2$ internal tides in the North Atlantic. See Figure 1b for location. (a) A snapshot internal tide field, showing a number of long-range internal tidal beams. (b) The time-latitude map of along-beam Greenwich phase from Cape Verde Island (14°55′N, 336°30′E). (c) As in Figure 5b but for one beam from the Great Meteor Seamount (331° 30′E, 30°N). In both panels, the red lines indicate co-phase lines, at intervals of one wavelength (≈150 km in space, 12.42 h in time). The tilting co-phase lines imply that the propagation speed increases (travel time decreases) from 1995 to 2014. (d) The S-R travel time change rate (blue line) along the Cape Verde beam. The shading indicates the 95% confidence interval. The green line indicates the bidecadal trend. The red line indicates the Argo measured OHC changes (with its 2005–2014 mean removed). A scaling (1% travel time change ≡ $0.7\times10^9$ J m$^{-2}$ OHC change) is explained in Figure 3. (e) As in Figure 5d but for the Great Meteor beam. The outlier is likely due to the small number of Argo floats in 2005.

The yearly time series of S-R travel times during 1995–2014 reveals remarkable interannual variability. The largest difference may be up to 5 h (Figure 4e). In El Niño years (e.g., 1997/1998 and 2005/2006), the internal tide travels faster, consistent with the pileup of warm water in this region. In 2000, the internal tide travels more slowly, corresponding to the negative OHC anomaly caused by La Niña. The time series of travel time changes is highly correlated with the El Niño–Southern Oscillation (ENSO) index (Figure 4e). This example confirms that the interannual variability of the phase of internal tides can be detected by satellite altimetry. No significant bidecadal trend is observed in this region (in contrast to the North Atlantic in section 3.2), in agreement with the Argo measurements in *Roemmich et al.* [2015].

The success of ITOT rests on ocean warming signals accumulating and amplifying over the long-range propagation of internal tides. Therefore, a 1% ocean warming signal will be amplified 10 times after the internal tide travels 1500 km in distance (≈10 tidal periods in time). As shown in Figure 4c, a speed change rate of 2.3% means an 8.3° change in phase (i.e., 360° times 2.3%) over one wavelength, which is barely above the 95% confidence level (about 5°). Fortunately, in the far field over 2000 km away, the phase difference is accumulated up to 120°, much greater than the 95% confidence level.

### 3.2. An Example in the North Atlantic

Figure 5 shows the southbound $M_2$ internal tides in the North Atlantic. The time-latitude maps of Greenwich phase along two internal tidal beams are given: One is from the Cape Verde Islands (Figure 5b), and the other is from the Great Meteor Seamount (Figure 5c). The co-phase lines show the internal tide's wave fronts at intervals of one wavelength. They tilt forward with propagation, implying that the internal tide's speed increases (travel time decreases) over 1995–2014 (Figures 5b and 5c).

Travel time changes can be calculated from the phase differences between 6°N (receiver) and 15°N (source) as shown in the co-phase chart (Figure 5b). Wiggles on co-phase lines near the generation sites are likely induced in the generation process, as observed near Hawaii [*Zilberman et al.*, 2011]. By taking the difference between source and receiver, we can eliminate any phase change induced in generation. Then the travel time change rate (in percentage) is obtained from the ratio of the travel time change to the total travel time. Figure 5d shows the travel time change rate along the Cape Verde beam. The rate along the Great Meteor beam is calculated following the same procedure (Figure 5e). The results show that the travel times have significant interannual variability, compared to the internal tide's 95% confidence intervals in phase (shading). In particular, significant bidecadal trends are obtained by linear fit (green lines). Both beams reveal that the travel times decrease by 1–2 h over the past two decades (the internal tide travels faster), suggesting that this part of the North Atlantic is warming.

The ITOT-derived bidecadal trends can be tested against the OHC changes measured by Argo floats. The red curves in Figures 5d and 5e show yearly OHC changes along their respective paths. For each curve, its 2005–2014 mean is removed. The Argo float measurements are downloaded from http://www.argo.net. A scaling (1% travel time change ≡ $0.7\times10^9$ J m$^{-2}$ OHC change) is explained in Figure 3. The ITOT and Argo observations agree well for both interannual variations and bidecadal trends. This example further confirms that ITOT is feasible and useful.

## 4. Advantages

ITOT offers a unique opportunity for monitoring global ocean warming by tracking long-range internal tides from satellite altimetry. It will complement the existing programs such as the Argo Program, the XBT network, and the OceanSITES Program. Because these observational techniques provide different aspects of ocean warming, the scientific community will benefit from complementary observing methods [*Abraham et al.*, 2013; *Riser et al.*, 2016]. ITOT has the following outstanding features.

1. *A global observing network.* The ubiquity of internal tides in the global ocean makes it possible to monitor ocean warming on a global scale. However, ITOT does not apply to regions where there are no internal tidal beams or internal tides are overwhelmed by mesoscale processes (Figure 1). It is expected that multifrequency ITOT will use four major tidal constituents ($M_2$, $S_2$, $O_1$, and $K_1$) and thus provide a better coverage of the global ocean.
2. *A long-term, cost-effective, environmentally friendly observing network.* Internal tides are powered by the astronomical tidal potential, and thus no cost is needed to maintain the internal tide's radiation sources. The only cost is to sample internal tides along known beams (Figure 1). Thanks to the altimeter satellites maintained by relevant agencies, ITOT does not require extra investment. The combination of satellite altimetry and tomography makes ITOT a cost-effective observational tool for global ocean warming. In addition, the natural source of internal tides implies that ITOT has no environmental issues, making it a green sustainable technique.
3. *Integrating over long-range internal tidal beams.* Similar to acoustic tomography, ITOT suppresses mesoscale perturbations by integrating over long-range internal tidal beams. For comparison, mesoscale perturbations are the main error sources in the Argo temperature measurements; therefore, a large number of Argo floats are needed to suppress mesoscale perturbations. In ITOT, the background noise is suppressed, and the ocean warming signal is accumulated and amplified (section 2.1).

4. *Full-water column information.* The propagation speed of internal tides is determined by the WKB-scaled stratification profile. Thus, the ITOT derived speed changes contain full-water column information. However, ITOT itself cannot distinguish the upper layer and deep-layer contributions. The ambiguity requires constraints from Argo and XBT measurements (section 2.2). It is expected that some useful information on abyssal ocean warming can be obtained by combining these observing techniques.

## 5. Future Work

A concept of ITOT for monitoring global ocean warming has proven feasible and useful. However, much work is needed to develop this technique from a *proof of concept* level to a *mature* level (refer to *Lindstrom et al.* [2012]). In particular, future work is needed to quantify the accuracy of this technique. First, the accuracy of the phase of internal tides should be assessed. Taking advantage of the currently available >20 years of satellite altimeter data (Figure 2), the phase of internal tides and its bidecadal trends will be obtained. The results are testable using overlapping internal tidal beams (refer to Figure 1). Internal tidal beams of opposite propagation directions are particularly useful, because the difference in travel times of opposite beams can be used to quantify the effect of ocean currents, similar to acoustic reciprocal tomography [*Munk et al.*, 1995]. Second, the accuracy of the conversion functions associated with unknown warming profiles should be assessed. A global map of conversion function will be constructed, taken into consideration that the warming profile is a function of location [e.g., *Levitus et al.*, 2012]. Importantly, the ITOT derived OHC product will be calibrated against Argo and XBT measurements. In addition, both the internal tide's speed and OHC can be directly computed from the Estimating the Circulation and Climate of the Ocean, Phase II (ECCO2) state estimate [*Menemenlis et al.*, 2005]; therefore, the results can be used to quantify the accuracy of ITOT.

**Acknowledgments**
The author thanks Peter Rhines, Eric D'Asaro, and Carl Wunsch for their insightful suggestions. Peter Rhines suggested the concept of tomography using internal tides. Eric D'Asaro suggested the term internal tide oceanic tomography (ITOT). Suggestions and comments from Carl Wunsch greatly improved the manuscript. Discussions with Gregory Johnson, Eric Lindstrom, and Doug Luther helped develop the concept. The author thanks Cimarron Wortham and Leah Johnson for proofreading the manuscript. The Argo data were collected and made freely available by the International Argo Program and the national initiatives that contribute to it (http://www.argo.net). Argo is a program of the Global Ocean Observing System (GOOS). The satellite altimeter products were produced by Ssalto/Duacs and distributed by AVISO, with support from CNES (http://www.aviso.altimetry.fr). The World Ocean Atlas 2013 was produced and made available by NOAA's National Oceanographic Data Center (https://www.nodc.noaa.gov/OC5/woa13/). The internal tide and ocean heat content products presented in this study are available upon request (zzhao@apl.washington.edu). This work was supported by NSF and NASA.

## References

Abraham, J. P., et al. (2013), A review of global ocean temperature observations: Implications for ocean heat content estimates and climate change, *Rev. Geophys.*, *51*, 450–483, doi:10.1002/rog.20022.

Cazenave, A., H.-B. Dieng, B. Meyssignac, K. von Schuckmann, B. Decharme, and E. Berthier (2014), The rate of sea-level rise, *Nat. Clim. Change*, *4*(5), 358–361, doi:10.1038/nclimate2159.

Dushaw, B. D., B. M. Howe, B. D. Cornuelle, P. F. Worcester, and D. S. Luther (1995), Barotropic and baroclinic tides in the central North Pacific ocean determined from long-range reciprocal acoustic transmissions, *J. Phys. Oceanogr.*, *25*(4), 631–647.

Dushaw, B. D., et al. (2009a), A decade of acoustic thermometry in the North Pacific Ocean, *J. Geophys. Res.*, *114*, C07021, doi:10.1029/2008JC005124.

Dushaw, B. D., et al. (2009b), A global ocean acoustic observing network, in *Proceedings of OceanObs'09: Sustained Ocean Observations and Information for Society*, vol. 2, pp. 279–291, European Space Agency, Venice, Italy.

Gill, A. E. (1982), *Atmosphere-Ocean Dynamics*, 662 pp., Acad. Press, New York.

Johnson, G. C., and J. M. Lyman (2014), Oceanography: Where's the heat?, *Nature Clim. Change*, *4*(11), 956–957, doi:10.1038/nclimate2409.

Kosaka, Y., and S.-P. Xie (2013), Recent global-warming hiatus tied to equatorial Pacific surface cooling, *Nature*, *501*, 403–407, doi:10.1038/nature12534.

Legler, D. M., H. J. Freeland, R. Lumpkin, G. Ball, M. J. McPhaden, S. North, R. Crowley, G. J. Goni, U. Send, and M. A. Merrifield (2015), The current status of the real-time in situ Global Ocean Observing System for operational oceanography, *J. Oper. Oceanogr.*, *8*(S2), s189–s200, doi:10.1080/1755876X.2015.1049883.

Levitus, S., et al. (2012), World ocean heat content and thermosteric sea level change (0–2000 m), 1955–2010, *Geophys. Res. Lett.*, *39*(10), L10603, doi:10.1029/2012GL051106.

Liang, X., C. Wunsch, P. Heimbach, and G. Forget (2015), Vertical redistribution of oceanic heat content, *J. Clim.*, *28*(9), 3821–3833, doi:10.1175/JCLI-D-14-00550.1.

Lindstrom, E., J. Gunn, A. Fischer, A. McCurdy, and L. K. Glover (2012), A framework for ocean observing, in *Prepared for the Task Team for an Integrated Framework for Sustained Ocean Observing (IFSOO)*, IOC/INF–1284, UNESCO, Paris., doi:10.5270/OceanObs09-FOO.

Lyman, J. M., S. A. Good, V. V. Gouretski, M. Ishii, G. C. Johnson, M. D. Palmer, D. M. Smith, and J. K. Willis (2010), Robust warming of the global upper ocean, *Nature*, *465*, 334–337, doi:10.1038/nature09043.

Meehl, G. A., J. M. Arblaster, J. T. Fasullo, A. Hu, and K. E. Trenberth (2011), Model-based evidence of deep-ocean heat uptake during surface-temperature hiatus periods, *Nat. Clim. Change*, *1*(7), 360–364, doi:10.1038/nclimate1229.

Menemenlis, D., et al. (2005), NASA supercomputer improves prospects for ocean climate research, *EOS Trans. AGU*, *86*, 89–96, doi:10.1029/2005EO090002.

Munk, W., and P. F. Worcester (1976), Monitoring the ocean acoustically, in *Science, Technology, and the Modern Navy, Thirtieth Anniversary, 1946–1976*, edited by E. I. Salkovitz, pp. 497–508, Office of Naval Research, Arlington, VA.

Munk, W., F. Snodgrass, and M. Winbush (1970), Tides off-shore: Transition from California coastal to deep-sea waters, *Geophys. Fluid Dyn.*, *1*, 161–235.

Munk, W. H., and A. M. Forbes (1989), Global ocean warming: An acoustic measure?, *J. Phys. Oceanogr.*, *19*, 1765–1778.

Munk, W. H., P. F. Worcester, and C. Wunsch (1995), *Ocean Acoustic Tomography*, Cambridge Univ. Press, New York.

Purkey, S. G., and G. C. Johnson (2010), Warming of global abyssal and deep southern ocean waters between the 1990s and 2000s: Contributions to global heat and sea level rise budgets, *J. Clim.*, *23*, 6336–6351, doi:10.1175/2010JCLI3682.1.

Ray, R. D., and G. T. Mitchum (1996), Surface manifestation of internal tides generated near Hawaii, *Geophys. Res. Lett.*, *23*(16), 2101–2104.

Riser, S. C., et al. (2016), Fifteen years of ocean observations with the global Argo array, *Nat. Clim. Change*, *6*, 145–153, doi:10.1038/NCLIMATE2872.

Roemmich, D., G. C. Johnson, S. Riser, R. Davis, J. Gilson, W. B. Owens, S. L. Garzoli, C. Schmid, and M. Ignaszewski (2009), The Argo program: Observing the global ocean with profiling floats, *Oceanography*, *22*, 34–43, doi:10.5670/oceanog.2009.36.

Roemmich, D., J. Church, J. Gilson, D. Monselesan, P. Sutton, and S. Wijels (2015), Unabated planetary warming and its ocean structure since 2006, *Nat. Clim. Change*, *5*, 240–245, doi:10.1038/NCLIMATE2513.

Wunsch, C., and P. Heimbach (2014), Bidecadal thermal changes in the abyssal ocean, *J. Phys. Oceanogr.*, *44*, 2013–2030, doi:10.1175/JPO-D-13-096.1.

Zhao, Z. (2016), Using CryoSat-2 altimeter data to evaluate $M_2$ internal tides observed from multisatellite altimetry, *J. Geophys. Res. Oceans*, *121*, 5164–5180, doi:10.1029/2016JC011805.

Zhao, Z., M. H. Alford, J. B. Girton, L. Rainville, and H. L. Simmons (2016), Global observations of open-ocean mode-1 $M_2$ internal tides, *J. Phys. Oceanogr.*, *46*, 1657–1684, doi:10.1175/JPO-D-15-0105.1.

Zilberman, N. V., M. A. Merrifield, G. S. Carter, D. S. Luther, M. D. Levine, and T. J. Boyd (2011), Incoherent nature of $M_2$ internal tides at the Hawaiian Ridge, *J. Phys. Oceanogr.*, *41*(11), 2021–2036, doi:10.1175/JPO-D-10-05009.1.